

Enhanced Transmission through Squeezed Modes in a Self-Cladding Magnonic Waveguide

G. Duerr,¹ K. Thurner,¹ J. Topp,² R. Huber,¹ and D. Grundler^{1,*}

¹*Physik Department, Lehrstuhl für Physik funktionaler Schichtsysteme, Technische Universität München, James-Frank-Straße 1, Garching b. München D-85747, Germany*

²*Institut für Angewandte Physik und Mikrostrukturforschungszentrum, Universität Hamburg, Jungiusstraße 11, Hamburg 20355, Germany*

(Received 16 February 2012; published 29 May 2012)

We study spin-wave propagation in 360-nm wide Ni₈₀Fe₂₀ nanowires using all-electrical spin-wave spectroscopy. Creating a zigzag-like magnetization state, we find enhanced spin-wave transmission compared to the states of more homogeneous magnetization. Micromagnetic simulations show that the spin waves propagate in narrow channels, which in particular, are remotely positioned from the edges. The internal channels reflect field-controlled self-cladding. Interestingly, rotation of the magnetic field at a specific value is found to vary the propagation velocity without changing the eigenfrequency. This opens the perspective of the velocity modulation transistor following a concept known from semiconductor electronics.

DOI: [10.1103/PhysRevLett.108.227202](https://doi.org/10.1103/PhysRevLett.108.227202)

PACS numbers: 75.50.Bb, 75.30.Ds, 75.75.-c, 75.78.-n

Microwires and nanowires prepared from low-damping ferromagnetic metals have been recently studied as waveguides for spin waves (magnons) [1–15]. Such spin waves at GHz frequencies have wavelengths that are a few orders of magnitude shorter than the corresponding electromagnetic waves in free space. This feature allows one to create miniaturized microwave circuits, which might even be interconnected directly with spin electronics [16,17]. Considering the relatively large coherence length of spin waves, magnonic circuits such as magnonic cellular nonlinear networks have been predicted to provide advanced image processing and speech recognition capabilities based on the parallel processing of information [18]. Novel functionalities are thus suggested to follow from magnonics research [19,20]. So far, spin-wave propagation has been explored for magnonic waveguides subject to magnetic fields H mainly applied in the longitudinal or strictly transverse in-plane direction. Different modes have been addressed, e.g., center and edge modes [4,7]. The boundary conditions due to dipolar pinning have not been found to enforce true nodes at the geometrical edges such that the center modes exhibit finite precession amplitudes at the edges [21]. The edges in real waveguides are rough and therefore could lead to unwanted scattering. Indeed, attenuation lengths of a few micrometers have been measured in narrow wires, which are smaller than those in plain films [7]. From photonic waveguiding, it is known that a graded refractive index (or permittivity) allows light to be “squeezed” to the inner part of a glass fiber. There, the boundaryless internal guiding suppresses scattering at rough surfaces and enhances the attenuation length. The invention of this so-called cladding has promoted substantially optical information technology [22]. In this Letter, we study spin-wave propagation through 360-nm wide Ni₈₀Fe₂₀ (permalloy) nanowires where we intentionally

create the previously reported zigzag-like magnetic state [23]. Our data reveal an enhanced transmission signal. Micromagnetic simulations show that the propagating mode is squeezed into two narrow channels that are remotely positioned from the geometrical edges. In addition, we show that the transmission characteristics and spin-wave velocity v_g can be modulated by the strength and orientation of an applied field \mathbf{H} . The observed characteristics might allow the concept of a velocity modulation transistor (VMT) to be implemented for spin waves, as has already been done for electrons [24].

In our study, arrays of permalloy wires were prepared on top of semi-insulating GaAs substrates using electron beam lithography and lift-off processing [25]. We report here on wires with $w = 360$ nm where the zigzag-like magnetic configuration was found to extend over the broadest field region. The wires were 25 ± 2 -nm thick. The edge roughness was about $\rho = 10$ nm (root-mean-square [rms] value). We studied approximately 350 nominally identical wires in parallel to enhance the signal-to-noise ratio (Fig. 1). The edge-to-edge separation was 540 nm to avoid magnetostatic and dynamic coupling [26]. The wire array was covered with a 4-nm thick sputtered SiO₂ isolation layer. On top of the isolation layer, two collinear coplanar waveguides (CPWs) tailored for all-electrical spin-wave spectroscopy were deposited using electron beam lithography and electron beam evaporation of Cr and Au. We label these waveguides CPW1 and CPW2, each consisting of ground-signal-ground leads. CPW1 (CPW2) is connected to port 1 (port 2) of a vector network analyzer, thus allowing experiments where spin waves are excited by CPW1 through the radio frequency magnetic field \mathbf{h}_{rf} , then travel along the propagation distance $d = 7.6 \mu\text{m}$, and are detected by CPW2. The phase shift acquired along d enters the scattering parameter

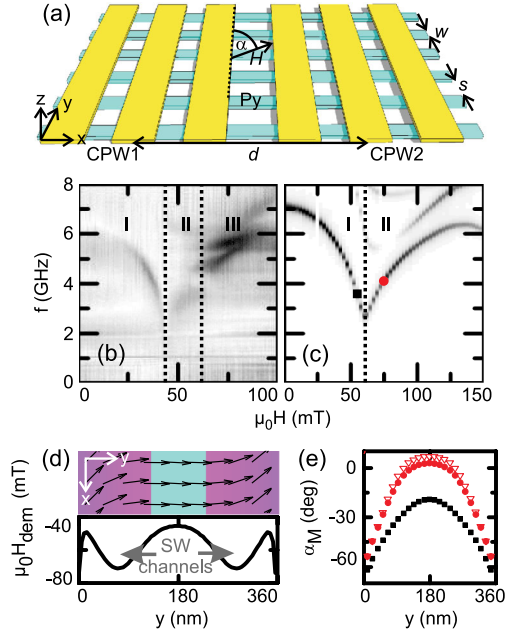


FIG. 1 (color online). (a) Sketch of nanowires underneath two collinear CPWs introducing the relevant parameters. (b) Spectroscopy data S_{11} taken at $\alpha = 2^\circ$. The field-dependent black contrast displays spin wave resonances. (c) Eigenfrequencies extracted from micromagnetic simulations at $\alpha = 2^\circ$ performed on ideal nanowires. Symbols mark where we evaluate α_M in (e). (d) Simulated zigzag magnetic configuration (top) and demagnetization field H_{dem} (bottom) in the wire along the y direction for $\alpha = 2^\circ$ at 75 mT. Fine arrows illustrate $M(x, y)$. Bright (dark) background color marks where $\alpha_M > 0$ (< 0). (e) Angle α_M for $\alpha = 2^\circ$ at 50 mT (squares) and 75 mT (circles), as well as $\alpha = 3.5^\circ$ at 75 mT (triangles) for comparison.

S_{21} and allows us to calculate the group velocity v_g of the spin wave [27–30]. The finite width of the CPWs of approximately 800 nm provoked a finite wave vector k along the nanowire in the x direction. The maximum excitation strength is near $k_{\text{CPW}} = 1.9 \times 10^4$ rad/cm. The coordinate system and orientation of \mathbf{H} is defined as follows [Fig. 1(a)]: The x axis is parallel to the wires' long axis (easy axis), the y axis is perpendicular to the wires in the sample plane, and the z axis is perpendicular to the sample plane. The angle α is defined with respect to the y axis. Simulations were performed using the geometrical parameters of the wires as listed above, but with $\rho = 0$. We took the saturation magnetization to be $M_{\text{sat}} = 775$ kA/m. A uniform simulation layer was used in the z direction considering a film thickness of 26 nm. Three sets of micromagnetic simulations were performed: quasistatic simulations, simulations for a wave vector $k = 0$ (uniform excitation), and simulations for $k > 0$ (non-uniform excitation). For $k = 0$, uniform excitation and 2D periodic boundary conditions (PBCs) were used. The simulated structure was 8 by 192 square-pixels large in the x and y directions, respectively, using a lateral cell size of

4.6875 nm per pixel. In the x direction (y direction), the simulated structure was $\Delta x = 37.5$ -nm (900-nm) long. Note that in the y direction, we simulated the 360-nm wide nanowire and the remaining vacuum gap with a width of 540 nm, as was consistent with the real sample [31]. A uniform excitation pulse was used to excite spin precession. After a simulation time of 6 ns, a fast Fourier transform (FFT) was performed of the time evolution of magnetization $\mathbf{M}(x, y, t)$ in order to obtain field-dependent eigenfrequencies. For simulations on excitations with wave vector $k > 0$, we considered $\Delta x = 9.6 \mu\text{m}$ in the x direction maintaining the 2D PBCs. The pulse had a rise and fall time of 0.025 ns and a duration of 0.05 ns. The pulse covered the entire simulated structure in the y direction and a 800-nm long segment in the x direction. The inhomogeneous field pulse stimulated a finite wave vector, k , parallel to the x direction, i.e., the propagation direction in the experiment. We analyzed a time period of 10 ns after the pulsed excitation. Subsequently a spatial and temporal FFT of the time-domain simulation data was performed in order to generate k -dependent spin-wave frequencies, i.e., a dispersion relation $f(k)$ [32]. Further details are given in Ref. [33]. The magnetic history was identical to the experimental conditions. For this Letter, we define the parameter α_M that measures the angle between a microscopic magnetic moment in the nanowire and the y axis.

In Fig. 1(b), field-dependent spectra are plotted as a grayscale graph. The magnetic history is as follows. The wires are saturated by $\mu_0 H = 100$ mT applied at $\alpha = -90^\circ$; i.e., the initial magnetization is in the negative x direction and α_M amounts to -90° for all moments. Then, the magnetic field is ramped down to zero. Subsequently, the field is ramped to the given field value at $\alpha = 2^\circ$. This means that for $H > 0$, the x component of the applied field H_x is antiparallel to the previous saturation field. We show the scattering parameter S_{11} measured in reflection configuration, i.e., CPW1 acts as an emitter and detector of spin waves. To further increase the signal-to-noise ratio, a reference data set taken at $\mu_0 H = 100$ mT and $\alpha = -90^\circ$ is subtracted where no spin-wave excitation takes place. The dark color represents absorption due to spin-wave excitation underneath CPW1. By S_{11} we probe different modes of the wires, i.e., standing and propagating ones. The field-dependent eigenfrequencies in Fig. 1(b) are consistent with the data obtained on similar but not identical nanowires in Ref. [23]. The simulated spectra shown in Fig. 1(c) remodel the field dependency. The main discrepancy remaining concerns the relevant magnetic fields needed to induce the different magnetic states. This discrepancy has been encountered before and it is attributed to the edge roughness parameter ρ , which is zero in the simulations but exhibits a rms value of 10 nm in the real nanowires [23]. We subdivide the measured spectra into three regimes I to III following Ref. [23]. In regime I, the central spins are destabilized. The eigenfrequency f of the

main mode decreases with H as the internal field decreases. The nanowires experience a switching process at about 45 mT and enter regime II [34]. Here, the magnetic moments at the two edges still point in the negative x direction as illustrated in Fig. 1(d), but the central moments have switched exhibiting $\alpha_M > 0$. Values of α_M extracted from simulations are shown in Fig. 1(e). At the center of the wire, α_M amounts to 2.7° (6.7°) for $\alpha = 2.0^\circ$ (3.5°) at 75 mT. Here, particularly, α_M is found to be larger than α . As a consequence, the nanowires exhibit the zigzag-like magnetic state as discovered in Ref. [23]. Only at large fields in regime III do the moments at the edges turn as well.

We now discuss the data obtained in transmission configuration where spin waves are excited at CPW1 and detected at CPW2. In Fig. 2(a), we depict the relevant scattering parameter S_{21} . The magnetic history is identical to Fig. 1(b). We present the real part of S_{21} . This signal incorporates the phase shift if both a spin wave propagates between CPW1 and CPW2, and the attenuation length

$$l_a = v_g \tau \quad (1)$$

is large enough to obtain a large signal-to-noise ratio (τ is the relaxation time). When l_a is large enough in relation to d , the real part exhibits contrast oscillations between black and white near a spin-wave resonance [30]. In Fig. 2(a), oscillations of the real part of S_{21} (inset) are detected in regime II when the zigzag state is present. They occur between about 2.5 and 4 GHz (highlighted by the dashed circle). The frequency difference Δf , defined in the inset of Fig. 2(a), is a measure of v_g according to [29] $v_g = 2\pi\Delta f/(2\pi/d) = d \cdot \Delta f$. In regimes I and III we do not resolve a contrast oscillation, i.e., the spin waves are attenuated too much before reaching CPW2. Strikingly, the modes in regimes I and III do not provide a clear

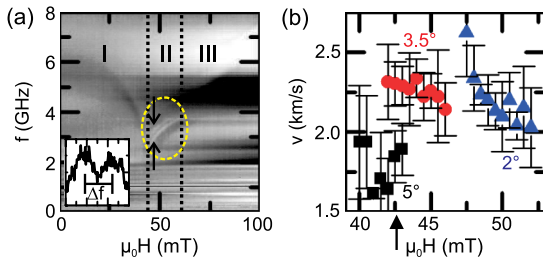


FIG. 2 (color online). (a) Real part of signal S_{21} measured at $\alpha = 2^\circ$ between emitter and detector CPW. The alternating black-white-black-white contrast in the dashed circle is attributed to phase shifts provoked by spin-wave propagation in regime II. Horizontal black and white stripes are artifacts from the CPWs. Inset: spectrum at 47.5 mT in the range from 2.8 to 3.4 GHz (indicated by arrows) showing an oscillating signal. Δf corresponds to a phase shift of 2π . (b) Propagation velocities at $\alpha = 5^\circ$ (squares), $\alpha = 3.5^\circ$ (circles), and $\alpha = 2^\circ$ (triangles). The arrow marks overlapping field regions (see text).

spin-wave propagation signal, whereas the spin waves in regime II do. Considering relative intensities $|S_{21}|/|S_{11}|$ measured at the same frequency of, e.g., 3.5 GHz, we find a signal in regime II that is increased by a factor of 2.5 relative to regime I.

Transmission experiments have been performed at three different angles $\alpha = 2^\circ$, 3.5° , and 5° where regime II existed. For all values of angle α , spin-wave propagation was resolved only in the zigzag state. For the three different angles, regime II existed in different field regions that partly overlapped. We extracted v_g from the contrast oscillations in both the real and imaginary parts (not shown) of S_{21} and S_{12} following Refs. [27,29]. We summarize the measured propagation velocities v_g in Fig. 2(b). The error bars reflect the variation of v_g from the independent data sets. For $\alpha = 2$ and 3.5° , the measured group velocities clearly decrease with increasing external field. Over a field range of 6 mT, v_g varies from about 2.6 to 2.0 km/s at $\alpha = 2^\circ$. Interestingly, below 45 mT, we find a small region (highlighted by the vertical arrow) where regime II exists at the two different angles $\alpha = 3.5$ and 5° for the same field H . In the simulations, considering the ideal nanowire, the overlapping field region is found to be even wider. Importantly, v_g varies with α by about 25% at the same H in Fig. 2(b). In a reference permalloy plain film (data not shown), group velocities decrease with increasing field as well. This is expected from the dispersion relation of the plain film. In the field regime from 40 to 55 mT, v_g is found to decrease from about 3.5 ± 0.5 km/s to 3 ± 0.5 km/s at $\alpha = 0^\circ$. The relative variation is smaller compared to the nanowires. In Ref. [17], a velocity of $v_g = 3.3$ km/s was reported for a spin wave excited in a thin permalloy film subject to an out-of-plane field of 0.6 T. Overall, the group velocities found here for the zigzag state in nanowires amount to values comparable to those of unpatterned thin films.

We now discuss spin-wave dispersion relations $f(k)$ to explain the experimentally observed differences in the transmission characteristics of regimes I and II. Simulation results for $\alpha = 2^\circ$ [Fig. 1(c)] show the characteristic minimum of the eigenfrequency at 57.5 mT, which marks the border between regimes I and II. To obtain the relevant dispersion relations $f(k)$ for regimes I and II, we consider field values of 50 and 75 mT, respectively. At 50 mT, i.e., in regime I, the slope $v_g = 2\pi\partial f/\partial k$ is found to be nearly zero in Fig. 3(a). Considering $v_g \approx 0$ in Eq. (1), the attenuation length is found to be nearly zero as well, explaining the lack of an oscillating contrast in Fig. 2(a). At slightly smaller H we obtain dispersion relations $f(k)$ (not shown) with small negative slopes. Such slopes are known from backward volume magneto-static waves, where the wave vector \mathbf{k} is considered to be parallel to \mathbf{M} . In Fig. 3(b) at 75 mT, i.e., in regime II, $f(k)$ is found to exhibit a positive slope. We extract $v_g = 2.1$ km/s. To illustrate the different propagation

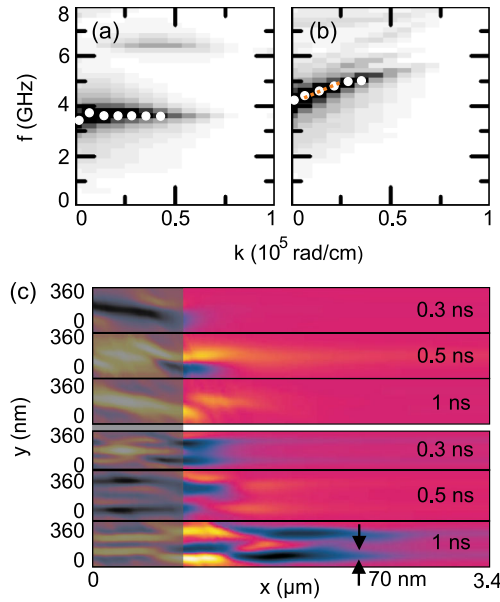


FIG. 3 (color online). Dispersion relations $f(k)$ extracted from micromagnetic simulations for $\alpha = 2^\circ$ at $\mu_0 H$ of (a) 50 (regime I) and (b) 75 mT (regime II). Dark color indicates a spin-wave resonance. White circles highlight maxima of the resonances. The broken line in (b) corresponds to $v_g = 2.1$ km/s. (c) Temporal evolution of the out-of-plane magnetization between 0.3 and 1 ns in regime I at $\mu_0 H = 50$ mT (three top rows) and in regime II at 75 mT (three bottom rows). Light (dark) color stands for negative (positive) spin-precession amplitude. The graphs have the same color coding. The field pulse h_{rf} excites a 800-nm wide area at the left end of the nanowire (gray area).

characteristics, we show the results of time-dependent simulations in Fig. 3(c) that were performed for 50 and 75 mT. Comparing the spatial distributions of spin-precession amplitudes after similar time periods, we find that spin excitations have propagated farther in regime II (75 mT) compared to regime I [35]. After 1 ns, the spin excitation has propagated more than $2 \mu\text{m}$ in regime II (bottom-most graph). Large spin-precession amplitudes are squeezed to two sub-100-nm channels. At the edges, the amplitudes are vanishingly small. In Ref. [23], it has been shown that the zigzag state gives rise to an inhomogeneous demagnetization field H_{dem} , creating two local minima of the internal field $H_{\text{int}} \cdot H_{\text{dem}}$ for $\alpha = 2^\circ$, and 75 mT is shown in Fig. 1(d). Each minimum supports a spin-wave nanochannel where spins are nearly perpendicular both to the exciting rf field \mathbf{h}_{rf} and to the wires' edges. In the nanochannels, Damon-Eshbach-like spin waves [36] are excited for which \mathbf{k} is perpendicular to \mathbf{M} . Such spin waves are known to exhibit a positive velocity v_g as seen in the dispersion $f(k)$ in Fig. 3(b) [37]. At the same time, the two local minima in Fig. 1(d) provoke a variation in the refractive index across the nanowire in the y direction [19]. This leads to the self-cladding effect for spin waves, i.e., the reduced spin-precession amplitudes at the geometrical

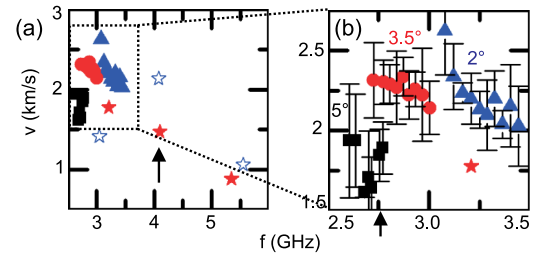


FIG. 4 (color online). (a) and (b) Propagation velocities summarized as a function of frequency f . We intentionally replot the data from Fig. 2(b) as a function of frequency f using the same symbols. Simulated data are for $\alpha = 2^\circ$ (open star) and $\alpha = 3.5^\circ$ (solid star). Arrows indicate where rotation of H varies the velocity v_g at the same f .

edges. In contrast to photonics, the cladding effect in magnonics is switched on and off by the magnetic field.

In Fig. 4(a), we compare the group velocities measured in regime II with simulations (stars). We find that regime II covers a broader range of eigenfrequencies for the simulations due to the discrepancy in experimental and simulated switching fields. The simulated velocity v_g is small for large values of the eigenfrequency f and, overall, increases with decreasing f . At small f , the simulated values v_g are in the same range as the experimental ones. Interestingly, both data sets, i.e., the simulated and measured ones, show that regime II supports spin waves of the same eigenfrequency but of different v_g when α is varied [highlighted by arrows in Figs. 4(a) and 4(b)] [38]. Thus, by rotating \mathbf{H} , the velocity is varied. The velocity modulation transistor has already been implemented for electrons in semiconductor devices [24]. Our findings suggest that a similar concept may apply to spin waves. Considering $\Delta v_g / \Delta \alpha$ as a figure of merit, we extract about $0.4 \text{ km}/(\text{s} \cdot \text{deg})$ and $0.3 \text{ km}/(\text{s} \cdot \text{deg})$ from the simulated and experimental data, respectively, in Fig. 4. The inhomogeneous spin configuration of the zigzag state is thus found to enhance the functionality [33] and opens perspectives for nano-optics with spin waves [7] on the sub-100-nm length scale.

In conclusion, we have found enhanced transmission of spin waves in permalloy nanowires when the zigzag-like magnetic state is formed. Due to self cladding, the spin-precession amplitude is reduced at the geometrical edges. We have shown that we can obtain a 25% modulation in group velocity in the zigzag state when the magnetic field is varied over an angle as small as 1.5° . We expect that future optimizations of the nanowires will lead to even larger modulation depths. The peculiar velocity modulation discovered here creates the potential for greater control in magnonics applications.

The authors thank J. E. Herriman for critically reading the manuscript, and S. Neusser for fruitful discussions and experimental support. Financial support by the German

Excellence Cluster Nanosystems Initiative Munich (NIM) is gratefully acknowledged. The authors thank for the support that was received from the European Community's Seventh Framework Programme under Grant No. 247556 NoWaPhen.

*grundler@ph.tum.de

- [1] M. Bailleul, D. Olligs, C. Fermon, and S. O. Demokritov, *Europhys. Lett.* **56**, 741 (2001).
- [2] M. Bailleul, D. Olligs, and C. Fermon, *Phys. Rev. Lett.* **91**, 137204 (2003).
- [3] R. Hertel, W. Wulfhekel, and J. Kirschner, *Phys. Rev. Lett.* **93**, 257202 (2004).
- [4] C. Bayer, J. P. Park, H. Wang, M. Yan, C. E. Campbell, and P. A. Crowell, *Phys. Rev. B* **69**, 134401 (2004).
- [5] S. Choi, K.-S. Lee, K. Y. Guslienko, and S.-K. Kim, *Phys. Rev. Lett.* **98**, 087205 (2007).
- [6] M. P. Kostylev, A. A. Serga, T. Schneider, T. Neumann, B. Leven, B. Hillebrands, and R. L. Stamps, *Phys. Rev. B* **76**, 184419 (2007).
- [7] V. E. Demidov, S. O. Demokritov, K. Rott, P. Krzyszczo, and G. Reiss, *Appl. Phys. Lett.* **92**, 232503 (2008).
- [8] V. Vlaminck and M. Bailleul, *Science* **322**, 410 (2008).
- [9] C. T. Boone, J. A. Katine, J. R. Childress, V. Tiberkevich, A. Slavin, J. Zhu, X. Cheng, and I. N. Krivorotov, *Phys. Rev. Lett.* **103**, 167601 (2009).
- [10] K. Vogt, H. Schultheiss, S. J. Hermsdoerfer, P. Pirro, A. A. Serga, and B. Hillebrands, *Appl. Phys. Lett.* **95**, 182508 (2009).
- [11] A. Kozhanov, D. Ouellette, Z. Griffith, M. Rodwell, A. P. Jacob, D. W. Lee, S. X. Wang, and S. J. Allen, *Appl. Phys. Lett.* **94**, 012505 (2009).
- [12] P. E. Roy, T. Trypiniotis, and C. H. W. Barnes, *Phys. Rev. B* **82**, 134411 (2010).
- [13] P. Pirro, T. Brächer, K. Vogt, B. Obry, H. Schultheiss, B. Leven, and B. Hillebrands, *Phys. Status Solidi B* **248**, 2404 (2011).
- [14] R. Lassalle-Balier and C. Fermon, *J. Phys. Conf. Ser.* **303**, 012008 (2011).
- [15] H. T. Nguyen, A. Akbari-Sharraf, and M. G. Cottam, *Phys. Rev. B* **83**, 214423 (2011).
- [16] V. E. Demidov, S. Urazhdin, and S. O. Demokritov, *Nature Mater.* **9**, 984 (2010).
- [17] M. Madami, S. Bonetti, G. Consolo, S. Tacchi, G. Carlotti, G. Gubbiotti, F. B. Mancoff, M. A. Yar, and J. Akerman, *Nature Nanotech.* **6**, 635 (2011).
- [18] A. Khitun, M. Bao, and K. L. Wang, *J. Phys. D* **43**, 264005 (2010).
- [19] S. Neusser and D. Grundler, *Adv. Mater.* **21**, 2927 (2009).
- [20] V. V. Kruglyak, S. O. Demokritov, and D. Grundler, *J. Phys. D* **43**, 264001 (2010).
- [21] K. Y. Guslienko, S. O. Demokritov, B. Hillebrands, and A. N. Slavin, *Phys. Rev. B* **66**, 132402 (2002).
- [22] C. K. Kao, Sand from centuries past: Send future voices fast, http://www.nobelprize.org/nobel_prizes/physics/laureates/2009/kao_lecture.pdf (2009).
- [23] J. Topp, J. Podbielski, D. Heitmann, and D. Grundler, *Phys. Rev. B* **78**, 024431 (2008).
- [24] H. Sakaki, *Jpn. J. Appl. Phys.* **21**, L381 (1982).
- [25] J. Topp, G. Duerr, K. Thurner, and D. Grundler, *Pure Appl. Chem.* **83**, 1989 (2011).
- [26] J. Topp, D. Heitmann, and D. Grundler, *Phys. Rev. B* **80**, 174421 (2009).
- [27] M. Bailleul, D. Olligs, and C. Fermon, *Appl. Phys. Lett.* **83**, 972 (2003).
- [28] M. Bao, K. Wong, A. Khitun, J. Lee, Z. Hao, K. L. Wang, D. W. Lee, and S. X. Wang, *Europhys. Lett.* **84**, 27009 (2008).
- [29] S. Neusser, G. Duerr, H. G. Bauer, S. Tacchi, M. Madami, G. Woltersdorf, G. Gubbiotti, C. H. Back, and D. Grundler, *Phys. Rev. Lett.* **105**, 067208 (2010).
- [30] V. Vlaminck and M. Bailleul, *Phys. Rev. B* **81**, 014425 (2010).
- [31] Applying the 2D periodic boundary conditions we did not restrict the simulations to 340 nanowires, but considered an infinite number.
- [32] V. Kruglyak and R. Hicken, *J. Magn. Magn. Mater.* **306**, 191 (2006).
- [33] G. Duerr, R. Huber, and D. Grundler, *J. Phys. Condens. Matter* **24**, 024218 (2012).
- [34] The upper field boundary of regime II was defined by the frequency gap observed in the low-frequency branch of the experimental data [23].
- [35] For both fields, we find a faint contrast change already at small times extending from the left to the right end. We attribute this to the extremely large phase velocity of spin waves exhibiting $f > 0$ at $k = 0$.
- [36] R. Damon and J. Eshbach, *J. Phys. Chem. Solids* **19**, 308 (1961).
- [37] We note that a wire with a *geometrical* width of 70 nm supports slow Damon-Eshbach-like spin waves of $v_g = 0.2$ km/s at 200 mT, which is needed to overcome the shape anisotropy field.
- [38] For a narrow spin-wave beam injected into an unpatterned film, the rotation of an applied field would vary the velocity as well. There, however, caustic effects may deflect the direction of the energy flow [39].
- [39] T. Schneider, A. A. Serga, A. V. Chumak, C. W. Sandweg, S. Trudel, S. Wolff, M. P. Kostylev, V. S. Tiberkevich, A. N. Slavin, and B. Hillebrands, *Phys. Rev. Lett.* **104**, 197203 (2010).